NANO LETTERS

Letter

pubs.acs.org/NanoLett

Quantifying Angular Correlations between the Atomic Lattice and the Superlattice of Nanocrystals Assembled with Directional Linking

Ivan A. Zaluzhnyy,[†,‡] Ruslan P. Kurta,[§] Alexander André,[∥] Oleg Y. Gorobtsov,[†] Max Rose,[†] Petr Skopintsev,[†,⊥] Ilya Besedin,[†,‡,#] Alexey V. Zozulya,[†,§] Michael Sprung,[†] Frank Schreiber,[∥] Ivan A. Vartanyants,[†,‡] and Marcus Scheele*[,∥]

[†]Deutsches Elektronen-Synchrotron DESY, Notkestraße 85, D-22607 Hamburg, Germany

[‡]National Research Nuclear University MEPhI (Moscow Engineering Physics Institute), Kashirskoe shosse 31, 115409 Moscow, Russia

[§]European XFEL GmbH, Holzkoppel 4, D-22869 Schenefeld, Germany

[∥]Eberhard Karls Universität Tübingen, Geschwister-Scholl-Platz, D-72074 Tübingen, Germany

Supporting Information

ABSTRACT: We show that the combination of X-ray scattering with a nanofocused beam and X-ray cross correlation analysis is an efficient way for the full structural characterization of mesocrystalline nanoparticle assemblies with a single experiment. We analyze several hundred diffraction patterns at individual sample locations, that is, individual grains, to obtain a meaningful statistical distribution of the superlattice and atomic lattice ordering. Simultaneous small- and wide-angle X-ray scattering of the same sample location allows us to determine the structure and orientation of the superlattice as well as the angular correlation of the first two Bragg peaks of the atomic lattices, their orientation with respect to the superlattice, and the average orientational misfit due to local structural disorder. This experiment is particularly advantageous for synthetic mesocrystals made by the simultaneous self-assembly of nanocrystals and surface-functionalization with conductive ligands. While the structural characterization of such materials has been challenging so far, the present method now allows correlating the mesocrystalline structure with optoelectronic properties.

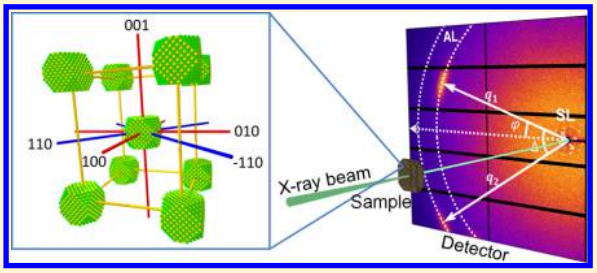

KEYWORDS: *Nanocrystals, self-assembly, mesocrystals, nanodiffraction, X-ray cross-correlation analysis*

Mesocrystals (MC) are three-dimensional arrays of iso-oriented single-crystalline particles with an individual size between 1 and 1000 nm.[1−5] Their physical properties are largely determined by structural coherence, for which the angular correlation between their individual atomic lattices and the underlying superlattice of nanocrystals (NC) is a key ingredient.[1,2] Colloidal NCs stabilized by organic surfactants have been shown to pose excellent building blocks for the design of synthetic MCs with tailored structural properties which are conveniently obtained by self-assembly of NCs from solution on a solid or liquid substrate by exploiting ligand−ligand interactions.[6−25] Typically, the utilized ligands consist of wide-gap, bulky hydrocarbons which render the MCs insulating.[26−33] MCs obtained in this way exhibit average grain sizes of ∼150 μm^2, which enables a detailed characterization by electron and/or X-ray microscopy.[34] Since the optoelectronic properties of PbS NC ensembles bear many opportunities for applications in solar cells or photodetectors, a number of ligand exchange procedures with small organic or inorganic molecules as well as single atom passivation strategies have been developed, all of which greatly increase the carrier mobilities within the SL of NCs.[28,33,35−44] Due to the short interparticle spacing imposed by these ligands, structural coherence is mostly lost in such superlattices, but in rare cases it has been demonstrated that significant long-range order and even mesocrystallinity can be preserved.[25,35,45] However, a persisting problem of these protocols is that they are prone to introduce defects in the superlattice structure with some degree of granularity and significantly smaller grain sizes, which poses difficulties in determining the angular correlation with a meaningful statistical distribution.[11,17,24,41,46,47] Using a conductive MC on the basis of PbS NCs,[35] we show how X-ray cross correlation analysis (XCCA)[48−52] in conjunction with a nanofocused X-ray beam can address this problem. Such a method should facilitate the application of synthetic conductive MCs with strong angular correlation for thermoelectrics, spintronics, (magneto-)electronics, and optics.[53−58]

Figure 1 displays a conductive MC of PbS NCs ligand-exchanged with the organic semiconductor tetrathiafulvalene-dicarboxylate TTFDA.[35] While Figure 1a−b demonstrates the typical dimensions of an individual MC grain (1−10 μm^2) and the high degree of order within the grain, a comparison of the

Received: February 11, 2017
Revised: May 8, 2017
Published: May 9, 2017

DOI: 10.1021/acs.nanolett.7b00584
Nano Lett. 2017, 17, 3511−3517

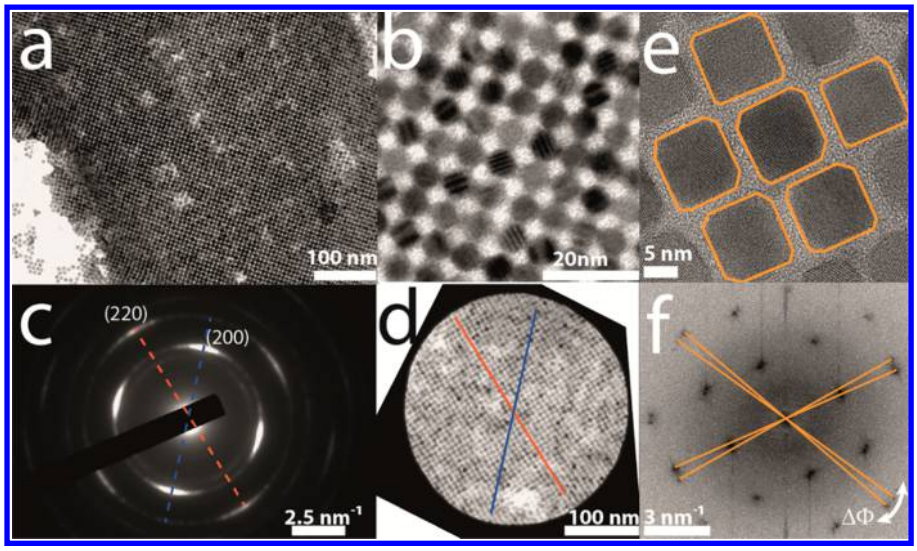

Figure 1. Electron micrographs of typical MCs, obtained with 6.2 nm PbS NCs cross-linked with tetrathiafulvalenedicarboxylate (TTFDA). (a) Low-magnification and (b) high-magnification micrograph of a typical grain showing the high degree of order in the superlattice. (c) Electron diffraction from the selected area displayed in (d) where red and blue lines indicate mutual directions in the AL (c) and SL (d). (e) High-resolution micrograph of a monolayer of a similar sample (10.7 nm PbS NCs) prepared under identical conditions. Boundaries of individual nanocrystals are highlighted in orange to emphasize that their atomic lattices are not precisely parallel. (f) Corresponding fast Fourier transform (FFT) of the image in (e). The split peaks in the FFT, exhibiting an orientational disorder ($\Delta\Phi$) of approximately 5°, further support this finding. Note that here, reciprocal space is shown in units $1/\lambda$ as opposed to the q-space depicted in Figure 3 with units of $2\pi/\lambda$.

electron diffraction pattern (Figure 1c) with the corresponding real-space image (Figure 1d) illustrates the angular dependence (blue and red lines) between the atomic lattice (AL) and the superlattice (SL). Imaging of individual NCs (Figure 1e and f) reveals a small degree of misalignment between neighboring ALs, which gives rise to broadening of the diffraction peaks in Figure 1c. On this highly local scale with poor statistics, the orientational disorder—represented by an angle $\Delta\Phi$—is $\lesssim 5°$ (Figure 1f). This angle conveys an important information about the degree of directional linking between the NCs in an SL exerted by their ligand shells. While the distribution in size and shape of the NCs is a source for inherent misalignment in such MCs, it has been shown that differences in the ligand shell can also dramatically alter $\Delta\Phi$.[11] Quantifying $\Delta\Phi$ for individual MC grains with good statistics is therefore important and will be addressed in the following by nanodiffraction.

Due to the granularity in the sample, any macroscopic imaging technique with a meaningful statistical description of the whole sample will necessarily return the average orientation of all SLs and ALs.[4,47] For the given example, which is representative for state-of-the-art artificial, conductive MCs, this renders a determination of the angular correlation and orientational disorder within each MC grain practically impossible. To alleviate this problem, we measured X-ray nanodiffraction of an MC obtained with the same NCs under the same conditions as those displayed in Figure 1a–d. A nanofocused beam with a footprint of about 400 × 400 nm^2, which is smaller than a typical MC domain, was used. We utilized PbS NCs obtained by wet-chemical procedures[59] since their size distribution is relatively narrow (~5%) (see Methods in the Supporting Information for sample preparation details), and TTFDA was chosen as a conductive linker because tetrathiafulvalene derivatives have been shown to invoke field-effect mobilities on the order of 10^{-4} to 10^{-3} cm^2/(V s) in PbS ensembles.[35,44] However, we emphasize that the analysis described in this Letter is not limited to specific NC superlattices and is generally applicable to elucidate angular

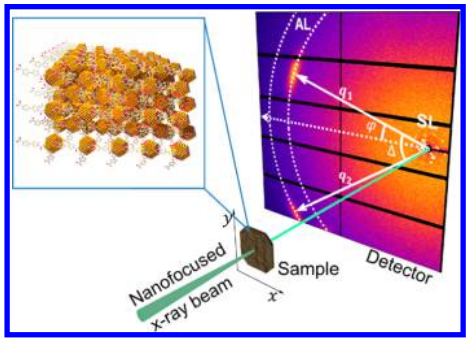

Figure 2. Scheme of the diffraction experiment. The sample is scanned by a nanofocused X-ray beam with the size of 400 nm × 400 nm in transverse direction. The detector is positioned downstream from the sample in transmission geometry and is shifted from the optical axis of the beam to measure simultaneously SL and AL peaks. The angle φ is measured with respect to the horizontal axis; the positive direction is counterclockwise, q_1 and q_2 are the magnitudes of the momentum transfer vectors, and $-\pi < \Delta \leq \pi$ is an angular variable. (inset) Details of the structure of the SL consisted of PbS NCs coated with TTFDA are shown.

correlations in MCs. The experiment schematically shown in Figure 2 (see Methods for experimental details) gave us a remarkable opportunity to simultaneously observe scattering from two distinct length scales (AL and SL) in a single image. This allowed us to determine the structure and orientation of the SL, as well as angular correlations between AL and SL within the same MC grain.

Typical diffraction patterns measured at different positions on the sample are shown in Figure 3, displaying up to four different orders of SL peaks in the small angle scattering (SAXS) region, with the momentum transfer values q_1^{SL} = 0.98 nm^{-1}, q_2^{SL} = 1.08 nm^{-1}, q_3^{SL} = 1.34 nm^{-1}, and q_4^{SL} = 1.72 nm^{-1}. As detailed in the Supporting Information, Figure S1, these scattering patterns can be fit to a body-centered tetragonal (bct) superlattice with some spatial fluctuations in the exact

DOI: 10.1021/acs.nanolett.7b00584
Nano Lett. 2017, 17, 3511−3517

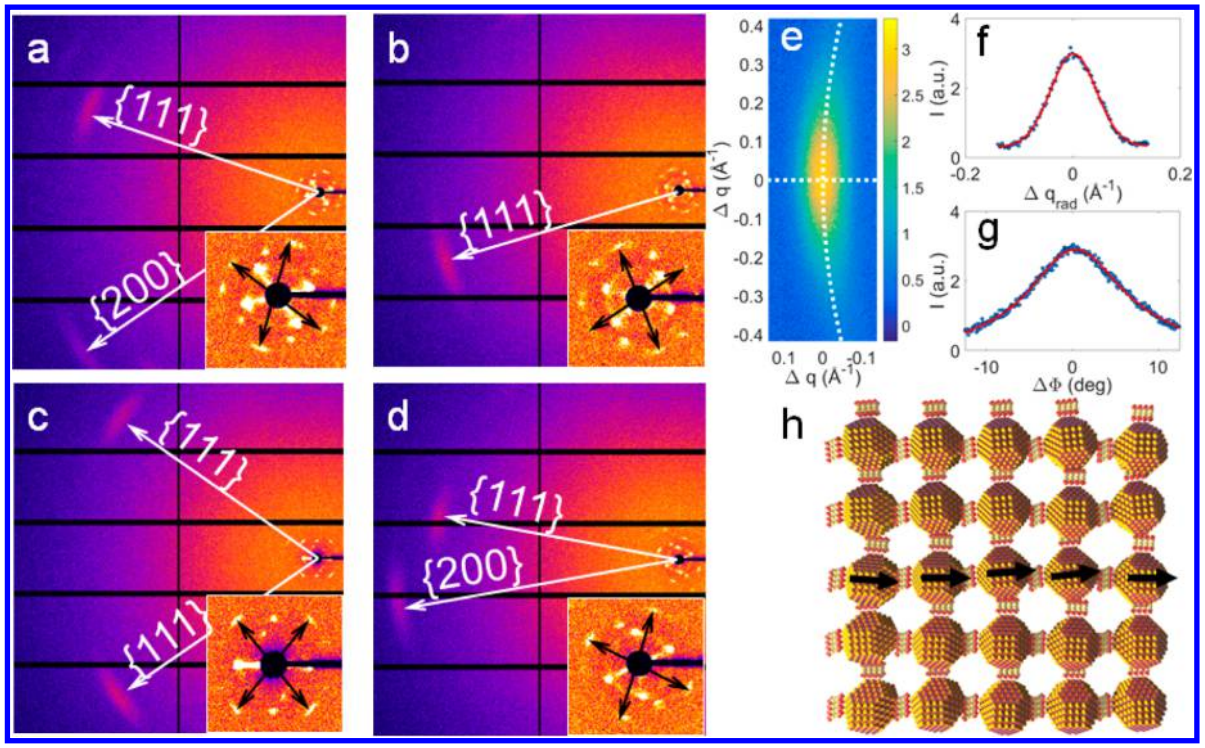

Figure 3. Examples of measured diffraction patterns from MCs. (a–d) Diffraction patterns measured at different positions of the sample. One can see SAXS scattering from the SL and Bragg peaks, corresponding to {111} and {200} reflections of the PbS AL. The insets display enlarged SAXS regions with the scattering signal from the SL. White arrows point to the Bragg reflections from the PbS AL, and black arrows show the diffraction peaks at q_4^{SL} = 1.72 nm^{-1} from the SL. (e) Two-dimensional shape of the 111 diffraction peak of the AL averaged over 412 diffraction patterns. White dashed lines represent cross sections in radial and azimuthal directions. (f–g) Radial and azimuthal cross section through the center of the peak, respectively. Points are experimental data, and red lines are Gaussian fits. (h) Idealized schematics of a PbS NC SL with a simulated orientational disorder of max. 10°. Black arrows indicate the same crystallographic direction in individual ALs. For clarity, the ligand spheres are sketched by small molecular stacks.

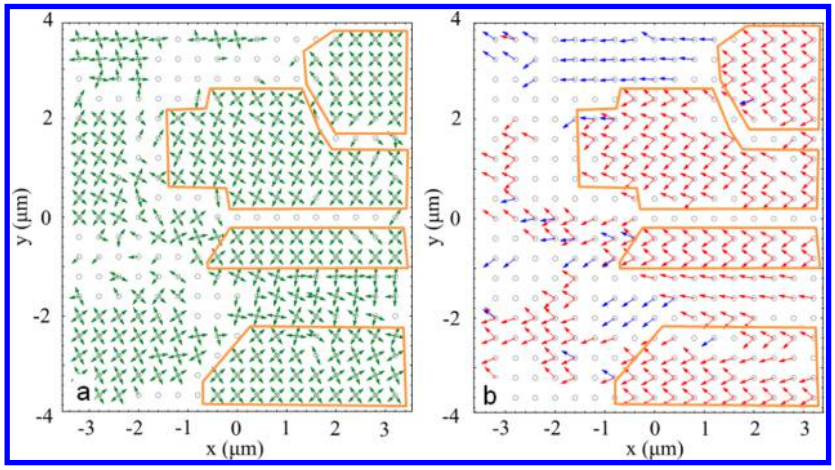

Figure 4. Spatially resolved maps of angular positions of the diffraction peaks. (a) Angular positions of diffraction peaks of the SL at q_4^{SL} are shown by green arrows. (b) Angular positions of {111} Bragg reflections at q_{111}^{AL} are shown by red arrows, and angular positions of {200} Bragg reflections at q_{200}^{AL} are shown by blue arrows. Domains are indicated by orange lines.

lattice parameters. We also often observed wide-angle X-ray scattering (WAXS) from the {111} and {200} planes of the AL at q_{111}^{AL} = 18.3 nm^{-1} and q_{200}^{AL} = 21.2 nm^{-1}, respectively. At some positions of the sample, we observed two AL {111} peaks (see Figure 3c). The presence of two {111} reflections originating from well-aligned NCs allowed us to unambiguously determine the orientation of AL. We scanned a sample area of 13.6 × 20 μm^2 in steps of 400 nm and recorded 1785 individual diffraction patterns, 412 of which displayed at least one well-resolved 111_{AL} diffraction peak. To obtain a statistical description of misorientation angle $\Delta\Phi$, we averaged the signal of all 111_{AL} diffraction peaks of the AL (Figure 3e), which allowed us to extract the radial and azimuthal cross section of the averaged diffraction peak shown in Figure 3f and g, respectively. We find that both cross sections are well-fit by Gaussian functions and that the peak is significantly broader in azimuthal than in radial direction. Attributing this additional azimuthal broadening to the orientational disorder of NCs

DOI: 10.1021/acs.nanolett.7b00584
Nano Lett. 2017, 17, 3511–3517

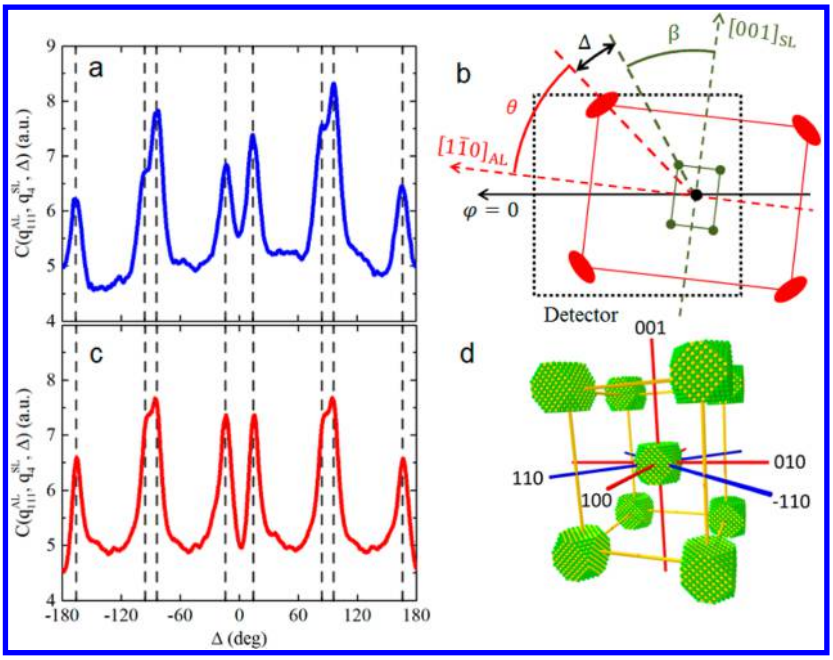

Figure 5. Angular correlations between AL and SL. (a) Average CCF calculated from the experimental data. (b) Schematic representation of AL and SL in reciprocal space. Red ellipsoids represent $\{111\}_{AL}$ reflections from the AL oriented in such a way that the $[110]_{AL}$ direction is perpendicular to the sample surface. The angle $\theta = \arctan(1/\sqrt{2}) \approx 35.26°$ between $[1\bar{1}0]_{AL}$ and $[1\bar{1}1]_{AL}$directions is fixed for the rock-salt lattice of PbS. Green circles represent $\{112\}_{SL}$ reflections from the SL oriented in such a way that the $[110]_{SL}$ direction is perpendicular to the sample surface. The value of the angle β between $[001]_{SL}$ and $[1\bar{1}2]_{SL}$ directions for the bct structure of the SL depends on the tetragonal distortion. To illustrate the meaning of Δ, the first angular correlation (for which $\Delta \approx 14°$) is shown. The area of reciprocal space covered by the detector is marked by a dashed rectangle. (c) Model CCF obtained assuming that the SL has tetragonal distortion $c/a = 1.22$. (d) Schematic of the MC unit cell displaying the angular correlation between AL and SL; collinear axes are indicated in red (⟨100⟩ directions) or blue (⟨110⟩ directions).

discussed above, we obtained a value of $\Delta\Phi \sim 10°$ (see Methods for details of evaluation). This—in contrast to Figure 1—represents the orientational disorder within a typical MC domain averaged over a macroscopic portion of the sample. Our result is illustrated in Figure 3h, depicting an SL of PbS NCs with a simulated $\Delta\Phi$ of 10°. Such rather large angular disorder may be rationalized as originating to a significant extent from the hybrid nature of the material, consisting of "hard" NCs and "soft" ligand spheres, which act as directional linkers between the NCs with some structural flexibility. Note that the real shape and binding mode of the ligand sphere may be more complex than that displayed in Figure 3h.

Furthermore, the large number of diffraction patterns allowed us to construct a spatially resolved map of the angular orientations of individual MC grains (Figure 4). It is apparent from Figure 4 that the sample is a granular MC with typical domain sizes of about 6−8 μm^2 (corresponding to at least 2×10^6 individual PbS particles in one domain), with well-resolved borders of width of about 0.5 μm between the domains with different orientations. The predominant orientation of the AL perpendicular to the sample surface is $[110]_{AL}$, deduced from the angle of 70.5° between two {111} reflections (the AL of PbS has rock-salt structure). For each position on the sample, we also determined a mismatch angle ψ displaying the azimuthal misorientation between SL and AL (see Supplementary Figure S3 for details). The mean value of this angle was $\psi = (0.1 \pm 2.5)°$, emphasizing that the angular correlation between SL and AL is very robust.

To determine the angular correlations and unit cell parameters within each domain quantitatively, we applied an XCCA approach (see Methods for XCCA details).[48−51,60−64] This method is based on the evaluation of a two-point angular cross-correlation function (CCF) that can be calculated for each diffraction profile as[48,49]

$$C(q_1, q_2, \Delta) = \langle I(q_1, \varphi) I(q_2, \varphi + \Delta) \rangle_\varphi \quad (1)$$

Here, we determined the CCF $C(q_{111}^{AL}, q_4^{SL}, \Delta)$ averaged over 412 diffraction patterns, for which scattering was observed both at q_{111}^{AL} and q_4^{SL}. These diffraction patterns correspond to sample positions where the $[110]_{AL}$ and $[110]_{SL}$ directions are perpendicular to the sample surface. In such a geometry, the full characterization of the sample's structure is possible by means of XCCA. The result of this analysis is shown in Figure 5a. We observed eight correlation peaks at $\Delta = \pm 14°$, ±84°, ±96°, and ±166°, representing the relative angles between q_{111}^{AL} and q_4^{SL}. In the following, we will show that the average CCF characterizes the structure of the MC, including the angular correlations between AL and SL. In the present case, the PbS AL has a rock-salt structure; its preferred orientation is $[110]_{AL}$ perpendicular to the film's surface, and geometric analysis of typical diffraction patterns suggests a bcc or bct lattice for the SL with predominant $[110]_{SL}$ orientation parallel to the same orientation of the AL. The symmetric profile of the CCF with respect to $\Delta = 0°$ also indicates collinearity of the $[001]_{SL}$ and $[001]_{AL}$ directions (see Methods for details). However, one can show that such two superimposed rock-salt and bcc lattices would be characterized by an average CCF with only six peaks at $\Delta = \pm 19.4°$, ±90°, ±160.6°, inconsistent with the eight peaks observed in our experiment. In contrast, we found that the experimental CCF can be reproduced if one considers a bct structure with the unit cell parameters $a = b \neq c$. For a bct lattice, the smallest angle $2\beta = 2 \arctan(c/a\sqrt{2})$ between two $[112]_{SL}$ directions is determined by the tetragonal distortion c/a and can be obtained by means of the CCF (see Figure 5b).

DOI: 10.1021/acs.nanolett.7b00584
Nano Lett. 2017, 17, 3511−3517

In this case, the CCF peaks appear at $\Delta = \pm(90° \pm \theta \pm \beta)$, where $\theta = 35.3°$ is the angle between the $[110]_{AL}$ and $[111]_{AL}$ directions of the rock-salt AL. Therefore, one can expect eight permutations for Δ in qualitative agreement with the CCF in Figure 5a. This way, a comparison with our experimental CCF in Figure 5a gave us value of $\beta \approx 40.7°$ and correspondingly a tetragonal distortion with $c/a \approx 1.22$.

To verify these findings, we modeled a CCF under the assumption of a rock-salt AL and bct SL with $c/a = 1.22$ and the alignment as detailed in Figure 5b (see Supporting Information for details of CCF modeling). The resulting model CCF shown in Figure 5c is in excellent agreement with the experimental CCF (Figure 5a) in terms of the positions and magnitudes of all eight peaks. We did not observe any additional broadening of the CCF peaks compared to the angular width of the diffraction peaks, which is further evidence of a strong angular correlation between the SL and AL. With respect to our main goal to elucidate the structure of the granular MC depicted in Figure 1, we find that the combination of nanodiffraction and XCCA demonstrated here is particularly powerful for the characterization of MCs with different symmetries of the AL and SL. In such a case, an unambiguous determination of the angular correlation requires the analysis of many grains in different orientations, since the number of collinear axes shared between the SL and AL is much smaller than for MCs where AL and SL have the same symmetry. This is illustrated in Figure 5d for the present case, which is directly derived from our XCCA, and features a total of five collinear axes shared between both lattices: all three ⟨100⟩ axes as well as the family of ⟨110⟩-directions. Note that there is no collinearity along the [011] direction or the family of ⟨111⟩ directions. The latter result is particularly noteworthy since the $\langle 111 \rangle_{SL}$ direction is the nearest-neighbor distance in a body-centered structure, and one may intuitively have expected an iso-orientation, which is not observed. While some of these collinearities have been described before (e.g., along the ⟨100⟩ axes), a full description of all angular correlations like that given in Figure 5d had remained elusive to date.[6,24] We note that the origin of the often-observed tetragonal distortion in PbS MCs and the role of the NC orientation is subject to ongoing discussions.[6,24,65,66] Some of the debated arguments in this respect include organic fibrillation, balanced contributions of ligand−ligand interactions from {100}- as well as {111}-facets, and kinetic arrest along the Bain path[6,46,65] from an fcc to a bcc structure. Since most previous studies focused on identifying collinearities between the AL and SL at the beginning (fcc) and the end (bcc) of the Bain path, this work attempts to contribute to the discussion by elucidating the angular correlations in the pivotal intermediate state (with bct structure). The fact that the cubic directions of the SL exhibit collinearity with the AL, and the <111> directions do not, supports the view that ligand−ligand interactions from specific facets of neighboring NCs are responsible for the tetragonal distortion.[24,65]

We note that the present study could also, in principle, be conducted by TEM-based electron diffraction (ED). However, the conventional approach of correlating wide-angle ED (to image the AL) with the Fourier transform of the bright-field image of the same area (to image the SL) faces serious challenges in this respect as it is hampered by the loss of structural information in the out-of-plane direction, which is inherent to such a two-dimensional imaging technique. More suitable are correlated ED studies at vastly different camera lengths to image both the AL and SL by ED only. In combination with the cross-correlation analysis used here, that technique is in fact the electron-based analogue to the method presented by us, which is based on X-rays. Within this comparison, X-rays are advantageous in the analysis of rather thick samples (due to the relatively large absorption cross-section for electrons) as well as for in situ measurements under ambient conditions or even different atmospheres for operando studies, since the method presented here does not require any reduced pressure.

We anticipate that the progressive exploration of synthetic MCs with increasing complexity, e.g., binary NC superlattices, nanorod assemblies, honeycomb lattices, etc. will benefit strongly from the present study. As we have demonstrated, a single experiment is sufficient to quantify the structure of the superlattice, its angular correlation with the atomic lattices, the average orientational disorder between atomic lattices, and a meaningful statistical distribution of these parameters as well as the length scale of the domains and their boundaries. This should greatly facilitate the understanding of structure−property relationships in MCs.

■ ASSOCIATED CONTENT

Supporting Information

The Supporting Information is available free of charge on the ACS Publications website at DOI: 10.1021/acs.nanolett.7b00584.

Description of the sample preparation, details of the X-ray scattering experiment, the X-ray cross-correlation analysis, the evaluation of the model cross-correlation function, and a comment on the effect of orientational disorder between atomic lattices. Figure S1: Analysis of the angular averaged signal in SAXS region. Figure S2: Evaluation of the angle 2β between two {112}SL peaks for the bct structure. Figure S3: Spatially resolved map of misorientation between the superlattice and atomic lattice. Figure S4: Illustration of the effect of atomic disorder in reciprocal space (PDF)

■ AUTHOR INFORMATION

Corresponding Author

*E-mail: marcus.scheele@uni-tuebingen.de.

ORCID

Marcus Scheele: 0000-0002-2704-3591

Present Addresses

⊥P.S.: Laboratory for Biomolecular Research, Paul Scherrer Institute, Villigen 5232, Switzerland.

#I.B.: National University for Science and Technology (MISiS), Leninskiy pr. 4, Moscow 119049, Russia.

Funding

This work was supported by the Virtual Institute VH-VI-403 of the Helmholtz Association as well as the DFG (SCHE1905/3; SCHE1905/4 and SCHR700/25).

Notes

The authors declare no competing financial interest.

■ ACKNOWLEDGMENTS

We acknowledge support by E. Weckert. We thank T. Salditt for providing nanofocusing instrument (GINIX) support at P10 beamline. High-resolution TEM imaging (Figure 1,e) and the synthesis of TTFDA were performed as user projects at the Molecular Foundry, which was supported by the Office of

DOI: 10.1021/acs.nanolett.7b00584
Nano Lett. 2017, 17, 3511−3517

Science, Office of Basic Energy Sciences, of the U.S. Department of Energy under Contract No. DE-AC02-05CH11231. We thank Mrs. Nadler for SEM measurements.

REFERENCES

(1) Bahrig, L.; Hickey, S. G.; Eychmüller, A. *CrystEngComm* **2014**, *16*, 9408−9424.
(2) Cölfen, H.; Antonietti, M. *Angew. Chem., Int. Ed.* **2005**, *44*, 5576−5591.
(3) Seto, J.; Ma, Y.; Davis, S. A.; Meldrum, F.; Gourrier, A.; Kim, Y.-Y.; Schilde, U.; Sztucki, M.; Burghammer, M.; Maltsev, S.; Jäger, C.; Cölfen, H. *Proc. Natl. Acad. Sci. U. S. A.* **2012**, *109*, 3699−3704.
(4) Simon, P.; Rosseeva, E.; Baburin, I. A.; Liebscher, L.; Hickey, S. G.; Cardoso-Gil, R.; Eychmüller, A.; Kniep, R.; Carrillo-Cabrera, W. *Angew. Chem., Int. Ed.* **2012**, *51*, 10776−10781.
(5) Song, R.-Q.; Cölfen, H. *Adv. Mater.* **2010**, *22*, 1301−1330.
(6) Bian, K.; Choi, J. J.; Kaushik, A.; Clancy, P.; Smilgies, D.-M.; Hanrath, T. *ACS Nano* **2011**, *5*, 2815−2823.
(7) Bodnarchuk, M. I.; Kovalenko, M. V.; Heiss, W.; Talapin, D. V. *J. Am. Chem. Soc.* **2010**, *132*, 11967−11977.
(8) Boles, M. A.; Engel, M.; Talapin, D. V. *Chem. Rev.* **2016**, *116*, 11220−11289.
(9) Boles, M. A.; Talapin, D. V. *J. Am. Chem. Soc.* **2014**, *136*, 5868−5871.
(10) Boneschanscher, M. P.; Evers, W. H.; Geuchies, J. J.; Altantzis, T.; Goris, B.; Rabouw, F. T.; van Rossum, S. A. P.; van der Zant, H. S. J.; Siebbeles, L. D. A.; Van Tendeloo, G.; Swart, I.; Hilhorst, J.; Petukhov, A. V.; Bals, S.; Vanmaekelbergh, D. *Science* **2014**, *344*, 1377−1380.
(11) Choi, J. J.; Bealing, C. R.; Bian, K.; Hughes, K. J.; Zhang, W.; Smilgies, D.-M.; Hennig, R. G.; Engstrom, J. R.; Hanrath, T. *J. Am. Chem. Soc.* **2011**, *133*, 3131−3138.
(12) Dong, A.; Chen, J.; Oh, S. J.; Koh, W.; Xiu, F.; Ye, X.; Ko, D.-K.; Wang, K. L.; Kagan, C. R.; Murray, C. B. *Nano Lett.* **2011**, *11*, 841−846.
(13) Dong, A.; Chen, J.; Vora, P. M.; Kikkawa, J. M.; Murray, C. B. *Nature* **2010**, *466*, 474−477.
(14) Evers, W. H.; Goris, B.; Bals, S.; Casavola, M.; de Graaf, J.; Roij, R.; Dijkstra, M.; Vanmaekelbergh, D. *Nano Lett.* **2013**, *13*, 2317−2323.
(15) Goodfellow, B. W.; Yu, Y.; Bosoy, C. A.; Smilgies, D.-M.; Korgel, B. A. *J. Phys. Chem. Lett.* **2015**, *6*, 2406−2412.
(16) Korgel, B. A.; Fullam, S.; Connolly, S.; Fitzmaurice, D. *J. Phys. Chem. B* **1998**, *102*, 8379−8388.
(17) Murray, C. B.; Kagan, C. R.; Bawendi, M. G. *Science* **1995**, *270*, 1335−1338.
(18) Nagel, M.; Hickey, S. G.; Frömsdorf, A.; Kornowski, A.; Weller, H. *Z. Phys. Chem.* **2007**, *221*, 427−437.
(19) Pietra, F.; Rabouw, F. T.; Evers, W. H.; Byelov, D. V.; Petukhov, A. V.; de Mello Donega, C.; Vanmaekelbergh, D. *Nano Lett.* **2012**, *12*, 5515−5523.
(20) Quan, Z.; Wu, D.; Zhu, J.; Evers, W. H.; Boncella, J. M.; Siebbeles, L. D. A.; Wang, Z.; Navrotsky, A.; Xu, H. *Proc. Natl. Acad. Sci. U. S. A.* **2014**, *111*, 9054−9057.
(21) Schliehe, C.; Juarez, B. H.; Pelletier, M.; Jander, S.; Greshnykh, D.; Nagel, M.; Meyer, A.; Förster, S.; Kornowski, A.; Klinke, C.; Weller, H. *Science* **2010**, *329*, 550−553.
(22) Shevchenko, E. V.; Ringler, M.; Schwemer, A.; Talapin, D. V.; Klar, T. A.; Rogach, A. L.; Feldmann, J.; Alivisatos, A. P. *J. Am. Chem. Soc.* **2008**, *130*, 3274−3275.
(23) Shevchenko, E. V.; Talapin, D. V.; Kotov, N. A.; O'Brien, S.; Murray, C. B. *Nature* **2006**, *439*, 55−59.
(24) Weidman, M. C.; Smilgies, D.-M.; Tisdale, W. A. *Nat. Mater.* **2016**, *15*, 775−781.
(25) Weidman, M. C.; Yager, K. G.; Tisdale, W. A. *Chem. Mater.* **2015**, *27*, 474−482.
(26) Chuang, C.-H. M.; Brown, P. R.; Bulović, V.; Bawendi, M. G. *Nat. Mater.* **2014**, *13*, 796−801.
(27) Kim, J.-Y.; Kotov, N. A. *Chem. Mater.* **2014**, *26*, 134−152.
(28) Kovalenko, M. V.; Scheele, M.; Talapin, D. V. *Science* **2009**, *324*, 1417−1420.
(29) Lee, J.-S.; Kovalenko, M. V.; Huang, J.; Chung, D. S.; Talapin, D. V. *Nat. Nanotechnol.* **2011**, *6*, 348−352.
(30) Scheele, M. *Z. Phys. Chem.* **2014**, *229*, 167−178.
(31) Scheele, M.; Brütting, W.; Schreiber, F. *Phys. Chem. Chem. Phys.* **2015**, *17*, 97−111.
(32) Talapin, D. V.; Lee, J.-S.; Kovalenko, M. V.; Shevchenko, E. V. *Chem. Rev.* **2010**, *110*, 389−458.
(33) Talapin, D. V.; Murray, C. B. *Science* **2005**, *310*, 86−89.
(34) Diroll, B. T.; Doan-Nguyen, V. V. T.; Cargnello, M.; Gaulding, E. A.; Kagan, C. R.; Murray, C. B. *ACS Nano* **2014**, *8*, 12843−12850.
(35) André, A.; Zherebetskyy, D.; Hanifi, D.; He, B.; Samadi Khoshkhoo, M.; Jankowski, M.; Chasse, T.; Wang, L.-W.; Schreiber, F.; Salleo, A.; Liu, Y.; Scheele, M. *Chem. Mater.* **2015**, *27*, 8105−8115.
(36) Choi, J.-H.; Fafarman, A. T.; Oh, S. J.; Ko, D.-K.; Kim, D. K.; Diroll, B. T.; Muramoto, S.; Gillen, J. G.; Murray, C. B.; Kagan, C. R. *Nano Lett.* **2012**, *12*, 2631−2638.
(37) Ip, A. H.; Thon, S. M.; Hoogland, S.; Voznyy, O.; Zhitomirsky, D.; Debnath, R.; Levina, L.; Rollny, L. R.; Carey, G. H.; Fischer, A.; Kemp, K. W.; Kramer, I. J.; Ning, Z.; Labelle, A. J.; Chou, K. W.; Amassian, A.; Sargent, E. H. *Nat. Nanotechnol.* **2012**, *7*, 577−582.
(38) Kagan, C. R.; Murray, C. B. *Nat. Nanotechnol.* **2015**, *10*, 1013−1026.
(39) Lauth, J.; Marbach, J.; Meyer, A.; Dogan, S.; Klinke, C.; Kornowski, A.; Weller, H. *Adv. Funct. Mater.* **2014**, *24*, 1081−1088.
(40) Law, M.; Luther, J. M.; Song, Q.; Hughes, B. K.; Perkins, C. L.; Nozik, A. J. *J. Am. Chem. Soc.* **2008**, *130*, 5974−5985.
(41) Luther, J. M.; Law, M.; Song, Q.; Perkins, C. L.; Beard, M. C.; Nozik, A. J. *ACS Nano* **2008**, *2*, 271−280.
(42) Nag, A.; Kovalenko, M. V.; Lee, J.-S.; Liu, W.; Spokoyny, B.; Talapin, D. V. *J. Am. Chem. Soc.* **2011**, *133*, 10612−10620.
(43) Scheele, M.; Engel, J. H.; Ferry, V. E.; Hanifi, D.; Liu, Y.; Alivisatos, A. P. *ACS Nano* **2013**, *7*, 6774−6781.
(44) Scheele, M.; Hanifi, D.; Zherebetskyy, D.; Chourou, S. T.; Axnanda, S.; Rancatore, B. J.; Thorkelsson, K.; Xu, T.; Liu, Z.; Wang, L.-W.; Liu, Y.; Alivisatos, A. P. *ACS Nano* **2014**, *8*, 2532−2540.
(45) Dong, A.; Jiao, Y.; Milliron, D. J. *ACS Nano* **2013**, *7*, 10978−10984.
(46) Choi, J. J.; Bian, K.; Baumgardner, W. J.; Smilgies, D.-M.; Hanrath, T. *Nano Lett.* **2012**, *12*, 4791−4798.
(47) Li, R.; Bian, K.; Hanrath, T.; Bassett, W. A.; Wang, Z. *J. Am. Chem. Soc.* **2014**, *136*, 12047−12055.
(48) Kam, Z. *Macromolecules* **1977**, *10*, 927−934.
(49) Wochner, P.; Gutt, C.; Autenrieth, T.; Demmer, T.; Bugaev, V.; Ortiz, A. D.; Duri, A.; Zontone, F.; Grübel, G.; Dosch, H. *Proc. Natl. Acad. Sci. U. S. A.* **2009**, *106*, 11511−11514.
(50) Altarelli, M.; Kurta, R. P.; Vartanyants, I. A. *Phys. Rev. B: Condens. Matter Mater. Phys.* **2010**, *82*, 104207−13.
(51) Kurta, R. P.; Altarelli, M.; Vartanyants, I. A. In *Advances in Chemical Physics*; John Wiley & Sons, Inc., 2016; pp 1−39.
(52) (a) Altarelli, M.; Kurta, R. P.; Vartanyants, I. A. X-ray cross-correlation analysis and local symmetries of disordered systems: General theory. *Phys. Rev. B: Condens. Matter Mater. Phys.* **2010**, *82*, 104207. (b) Altarelli, M.; Kurta, R. P.; Vartanyants, I. A. Erratum: X-ray cross-correlation analysis and local symmetries of disordered systems: General theory. *Phys. Rev. B* **2012**, *86* (17), 179904.
(53) Bird, J. P.; Akis, R.; Ferry, D. K.; Vasileska, D.; Cooper, J.; Aoyagi, Y.; Sugano, T. *Phys. Rev. Lett.* **1999**, *82*, 4691−4694.
(54) Chang, C. Y.; Fang, Y. K.; Sze, S. M. *Solid-State Electron.* **1971**, *14*, 541−550.
(55) Chen, G. *Phys. Rev. B: Condens. Matter Mater. Phys.* **1998**, *57*, 14958−14973.
(56) Matsui, H.; Tabata, H. *J. Appl. Phys.* **2006**, *99*, 124307.
(57) Peng, X.; Manna, L.; Yang, W.; Wickham, J.; Scher, E.; Kadavanich, A.; Alivisatos, A. P. *Nature* **2000**, *404*, 59−61.
(58) Qiao, J.; Kong, X.; Hu, Z.-X.; Yang, F.; Ji, W. *Nat. Commun.* **2014**, *5*, 4475.

DOI: 10.1021/acs.nanolett.7b00584
Nano Lett. 2017, 17, 3511−3517

(59) Weidman, M. C.; Beck, M. E.; Hoffman, R. S.; Prins, F.; Tisdale, W. A. *ACS Nano* **2014**, *8*, 6363−6371.
(60) Mendez, D.; Lane, T. J.; Sung, J.; Sellberg, J.; Levard, C.; Watkins, H.; Cohen, A. E.; Soltis, M.; Sutton, S.; Spudich, J.; Pande, V.; Ratner, D.; Doniach, S. *Philos. Trans. R. Soc., B* **2014**, *369*, 20130315.
(61) Kurta, R. P.; Grodd, L.; Mikayelyan, E.; Gorobtsov, O. Y.; Zaluzhnyy, I. A.; Fratoddi, I.; Venditti, I.; Russo, M. V.; Sprung, M.; Vartanyants, I. A.; Grigorian, S. *Phys. Chem. Chem. Phys.* **2015**, *17*, 7404−7410.
(62) Schroer, M. A.; Gutt, C.; Lehmkühler, F.; Fischer, B.; Steinke, I.; Westermeier, F.; Sprung, M.; Grübel, G. *Soft Matter* **2015**, *11*, 5465−5472.
(63) Mancini, G. F.; Latychevskaia, T.; Pennacchio, F.; Reguera, J.; Stellacci, F.; Carbone, F. *Nano Lett.* **2016**, *16*, 2705−2713.
(64) Zaluzhnyy, I. A.; Kurta, R. P.; Sulyanova, E. A.; Gorobtsov, A. Y.; Shabalin, A. G.; Zozulya, A. V.; Menushenkov, A. P.; Sprung, M.; Krówczyński, A.; Górecka, E.; Ostrovskii, B. I.; Vartanyants, I. A. Structural studies of the bond-orientational order and hexatic-smectic transition in liquid crystals of various compositions. *Soft Matter* **2017**, *13*, 3240−3252.
(65) Novak, J.; Banerjee, R.; Kornowski, A.; Jankowski, M.; Andre, A.; Weller, H.; Schreiber, F.; Scheele, M. *ACS Appl. Mater. Interfaces* **2016**, *8*, 22526−22533.
(66) Simon, P.; Bahrig, L.; Baburin, I. A.; Formanek, P.; Röder, F.; Sickmann, J.; Hickey, S. G.; Eychmüller, A.; Lichte, H.; Kniep, R.; Rosseeva, E. *Adv. Mater.* **2014**, *26*, 3042−3049.

DOI: 10.1021/acs.nanolett.7b00584
Nano Lett. 2017, 17, 3511−3517